Electronic Supplementary Material (ESI) for Journal of Materials Chemistry A.
This journal is © The Royal Society of Chemistry 2022

Near-infrared photothermally enhanced catalysis for benzene hydroxylation

Gengxin Wang, Bao Li* and Lixin Wu*

State Key Laboratory of Supramolecular Structure and Materials, College of Chemistry, Jilin University, Changchun 130012, P. R. China.

**E-mail: wulx@jlu.edu.cn; libao@jlu.edu.cn*

Table of Contents

S1. Materials

Cetyltrimethylammonium bromide (CTAB), sodium borohydride ($NaBH_4$), Chloroauric acid trihydrate ($HAuCl_4 \cdot 3H_2O$), silver nitrate ($AgNO_3$), ascorbic acid (AA), deuterium reagents (D_2O, DMSO-d_6, Methanol-d_4) used in experiments were purchased from Sigma-Aldrich.β-CD used in the present study was purchased from Aladdin and recrystallized three times before use. Benzene, phenol, benzoquinone, hydroquinone, p-toluene sulfonyl chloride (Ts-Cl), 2-(bromoethyl)-trimethylammonium bromide, potassium thioacetate, and 5,5-dimethyl-1-pyrroline N-oxide (DMPO) were the products of Aladdin. The thiourea, trichloroethylene, adamantane hydrochloride and other chemicals and solvents were commercially received from Beijing Chemical Reagent Industry. Water used in the experiment was doubly distilled. The Fenton reagent is prepared following the used ratio by adding H_2O_2 and $FeCl_3$ in aqueous solution.

S2. Measurements

^1H NMR and 1D NOSEY NMR spectra were conducted on a Bruker Avance 500 MHz NMR spectrometer by using tetramethylsilane (TMS) as an internal reference (δ = 0 ppm). MALDI-TOF mass spectra were recorded on an autoflex MALDI-TOF mass spectrometer (Bruker) equipped with a nitrogen laser (337 nm, 3 ns pulse). FT-IR spectra were carried out on a Bruker Vertex 80V FT-IR spectrometer. UV-vis spectra were recorded on a Varian CARY 50 Probe spectrometer with a 1 cm quartz cell. Transmission electronic microscopic (TEM) was conducted on a JEOL JEM 2100F under an accelerating voltage of 200 Kv without staining. The X-ray photoelectron spectroscopic (XPS) data are acquired on an ESCALAB-250 spectrometer with a monochromic X-ray source (Al Kα line, 1486.6 eV) and the charging shift was corrected at the binding energy of C(1s) at 284.6 eV. Inorganic elemental analysis was performed on a POEMS inductively coupled plasma atomic emission spectrometer (ICP-AES). The dynamic light scattering (DLS) and z-potential measurements were performed on a Zetasizer NanoZS instrument (Malvern Instruments). The electron paramagnetic resonance (EPR) spectra recorded on a Bruker E500 EPR spectrometer were used to detect the hydroxyl radical generated in the catalytic oxidation system with DMPO as the radical spin-trapped reagent. The high-performance liquid chromatography (HPLC) analysis was performed on a SHIMADZU LC-20A with an Aglient ZORBAX SB-C18 column (d = 5 μm, l = 250 mm) at 40°C. The eluent was methanol/H_2O (70:30) at a flow rate of 0.75 mL/min. The photothermal conversion experiments were carried out with an 808 nm laser light source and adjustable output power (Xi'an Hxrld laser Tech. Co., Ltd).

S3. Synthesis of the CD-AuNR.

The synthesis of T-CD follows the route shown in Scheme S1.

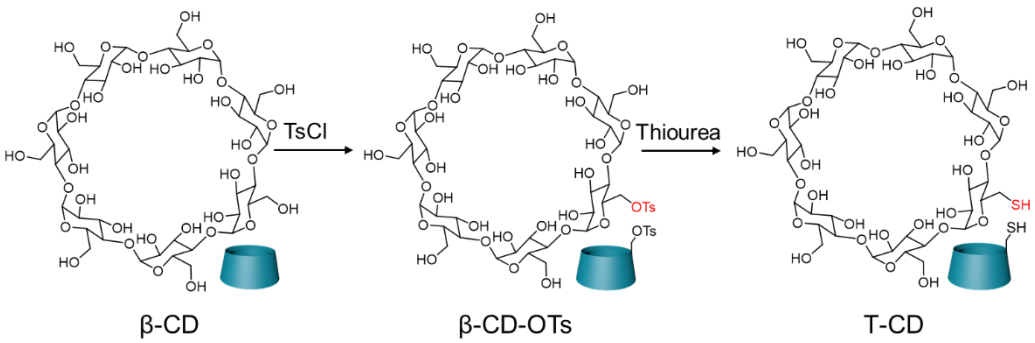

Scheme S1 The synthetic route of T-CD.

Synthesis of 6-TsO-β-cyclodextrin (β-CD-OTs). β-CD (30.0 g) was dissolved in 250 mL H_2O, getting a white turbid solution. Then, NaOH solution (10 mL, 8.21 mol/L) was added dropwise with stirring and a clear mixed solution was obtained finally. Ts-Cl (5.04 g, 26.43 mmol) that was dissolved in 15 mL of CH_3CN was added dropwise to the above solution. After stirring for 2 h at room temperature, the mixture was filtered and the filtrate was adjusted with 10% HCl to pH of 7–9, yielding white precipitate. After placing in a refrigerator at 5°C overnight, the precipitate was filtered and washed with acetone to obtain crude product. The solid was recrystallized from CH_3OH/H_2O = 1/1 mixed solvent three times and filtered to give pure product (4.7 g). ^{1}H NMR (500 MHz, DMSO-d_6) δ 7.76 (d, 2H), 7.44 (d, 2H), 5.98–5.53 (m, 14H), 5.01–4.69 (m, 14H), 4.58–4.08 (m, 9H), 3.80–3.39 (m, 32H), 2.44 (s, 3H). MALDI-TOF MS (m/z): 1312.2 [M+Na], 1328.2 [M+K].

Synthesis of 6-thio-β-cyclodextrin (T-CD). The above obtained β-CD-OTs (4.5 g) and thiourea (5.0 g, 65.8 mmol) were dissolved in 240 mL of methanol-water mixed solution (CH_3OH/H_2O in 4:1), and the solution was refluxed with stirring for 50 h. The solvent was removed by rotary evaporation under vacuum and then 60 mL of CH_3OH was added to the residue, filtering after 1.5 h of stirring. The obtained solid was redissolved in 140 mL of 10% NaOH aqueous solution, stirring at 50°C for 5 h. 10% HCl was then added to the mixture to adjust the pH to 2. 10 mL of trichloroethylene was added dropwise, stirred at room temperature for 24 h, filtered and washed with water and acetone to obtain a white solid. The crude product was recrystallized in water three times, filtered and dried under vacuum to obtain pure product T-CD (1.5 g). ^{1}H NMR (500 MHz, DMSO-d_6) δ 5.73 (s, 14H), 4.83 (s, 7H), 4.44 (s, 7H), 3.63 (s, 21H), 3.35 (s, 18H), 2.98 (s, 1H), 2.76 (s, 1H), 2.06 (s, 1H). MALDI-TOF MS (m/z): 1173.0 [M+Na], 1189.0 [M+K].

The synthesis of CD-AuNR follows the route in Scheme S2 and the procedures are described in the main text in detail.

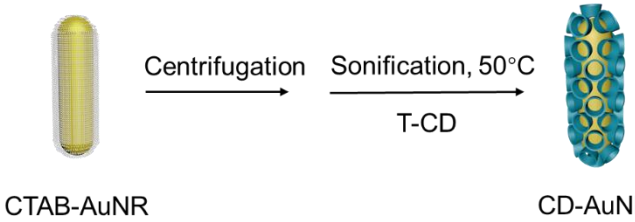

Scheme S2 The synthetic route of CD-AuNR.

S3. Characterization of CD-AuNR.

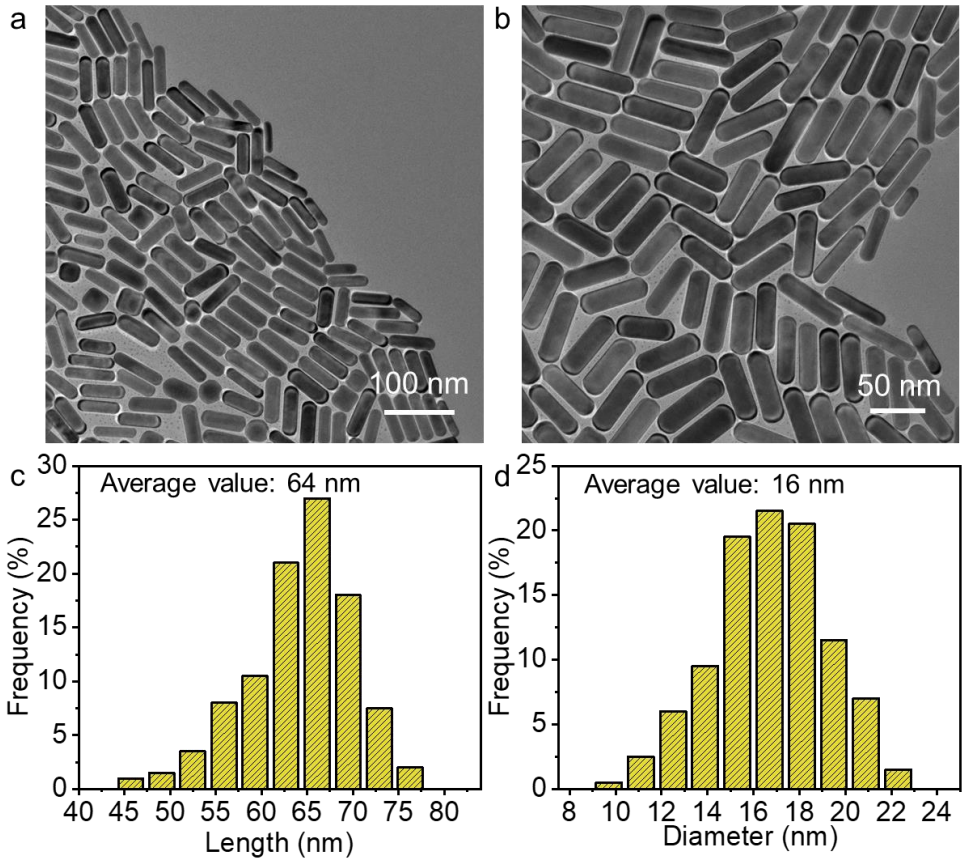

Fig. S1 (a) TEM image of CTAB-AuNR in water and (b) its local amplification with the statistic graphs of average (c) length in size and (d) diameter.

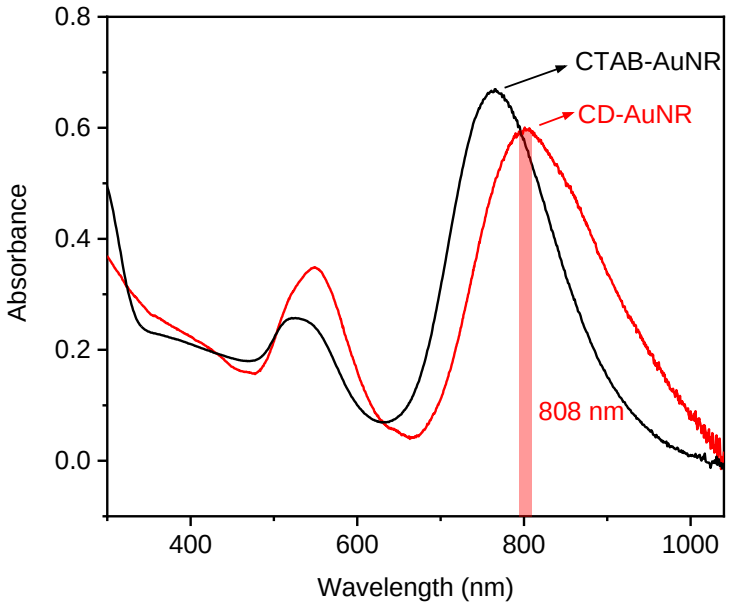

Fig. S2 UV-vis spectra of CTAB-AuNR (black) and CD-AuNR (red) in aqueous solution.

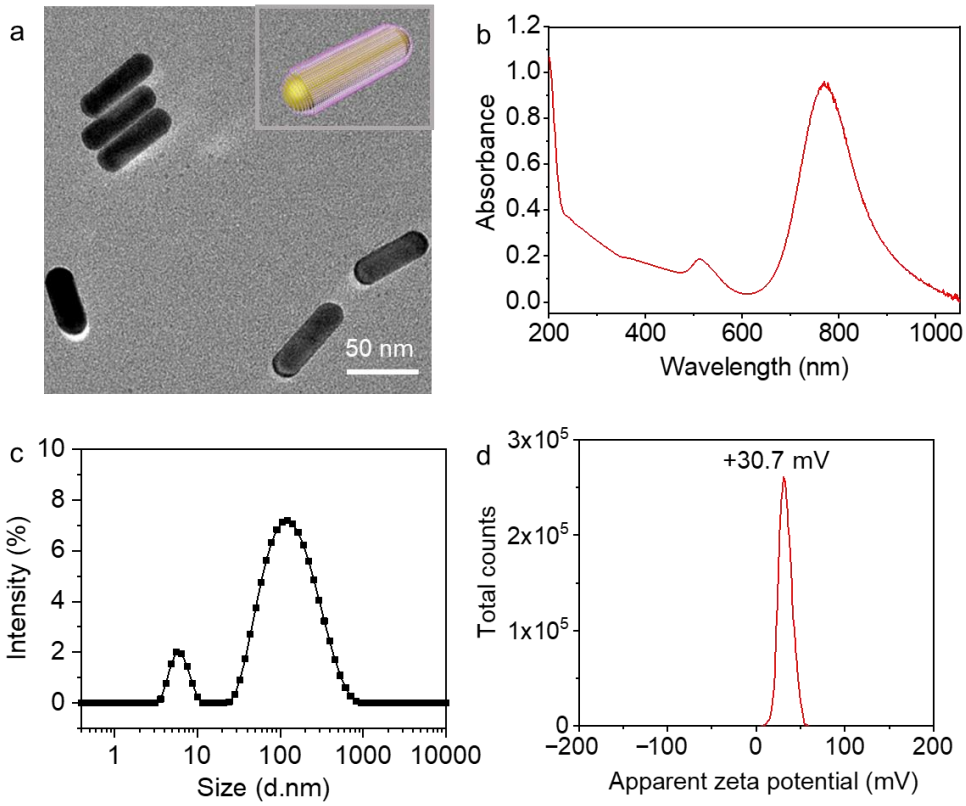

Fig. S3 (a) TEM image, (b) UV-vis spectrum, (c) DLS diagram, and (d) apparent zeta potential of cationically modified AuNRs (C-AuNR) in aqueous solution, where the inset in (a) represents the schematic drawing.

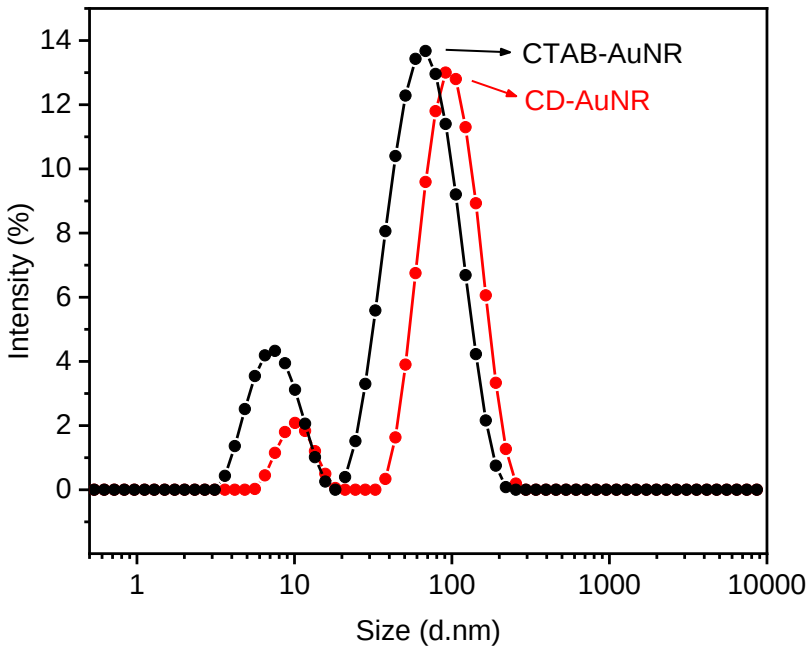

Fig. S4 DLS diagrams of CTAB-AuNR and CD-AuNR in water.

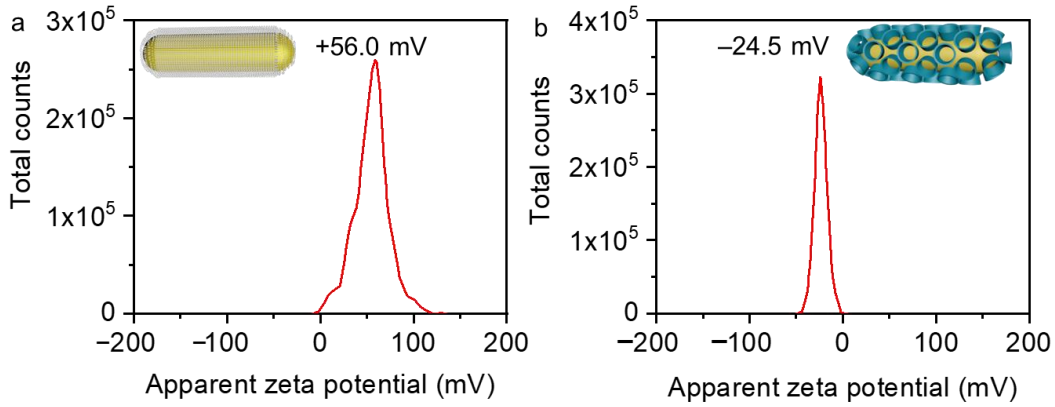

Fig. S5 Apparent zeta potentials of (a) CTAB-AuNR and (b) CD-AuNR in water.

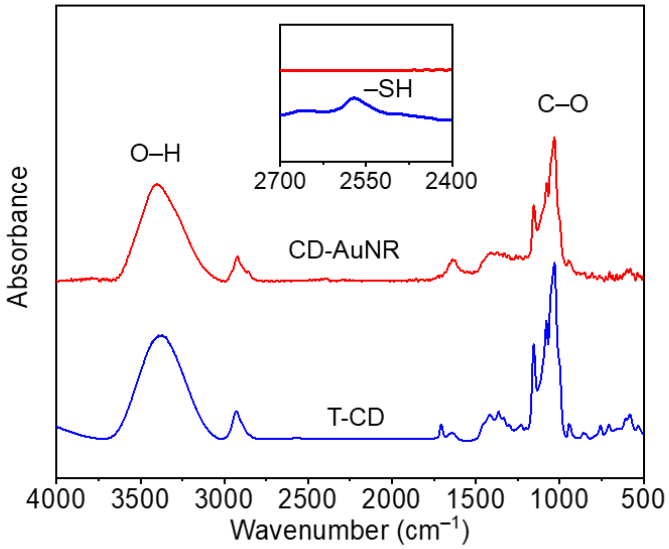

Fig. S6 FT-IR spectra of T-CD and CD-AuNR in KBr pellets.

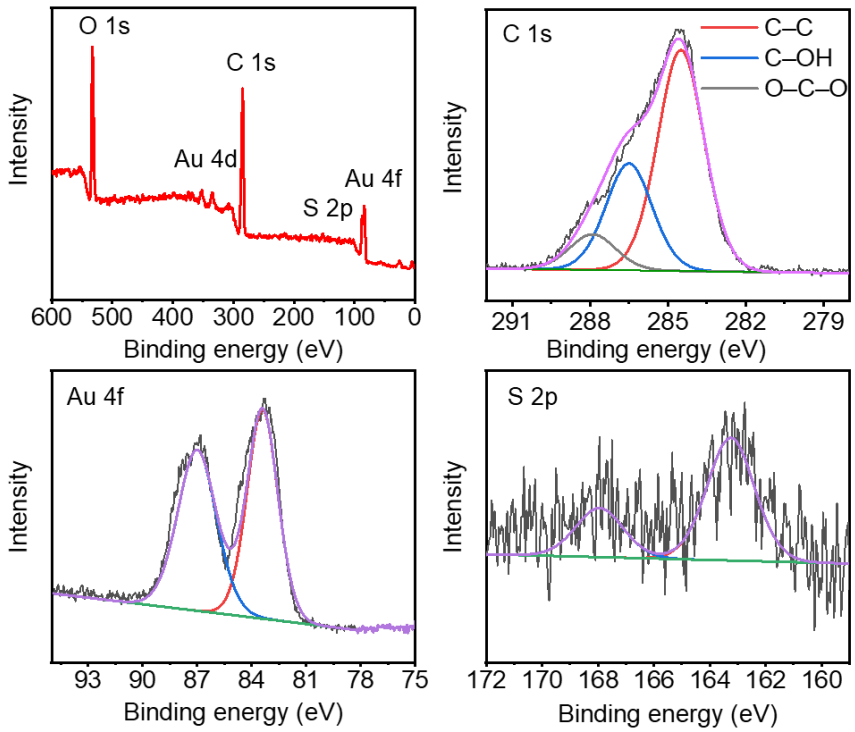

Fig. S7 XPS spectra of CD-AuNR.

S5. Calculation of CD coverage on AuNR.

From the statistics of TEM image shown in Fig. S1, AuNR occupies about 98.16% and can be described as a cachet model at an average total length of 64 nm with a half sphere in an average diameter of 16 nm at both ends. The remainder is about 1.12% of gold sphere with an average diameter of 2.0 nm. Based on the published structure of β-CD, the height is about 0.79 nm and the outer diameter at the secondary face is 1.53 nm.[1, 2] The structures are shown in Scheme S3a−c.

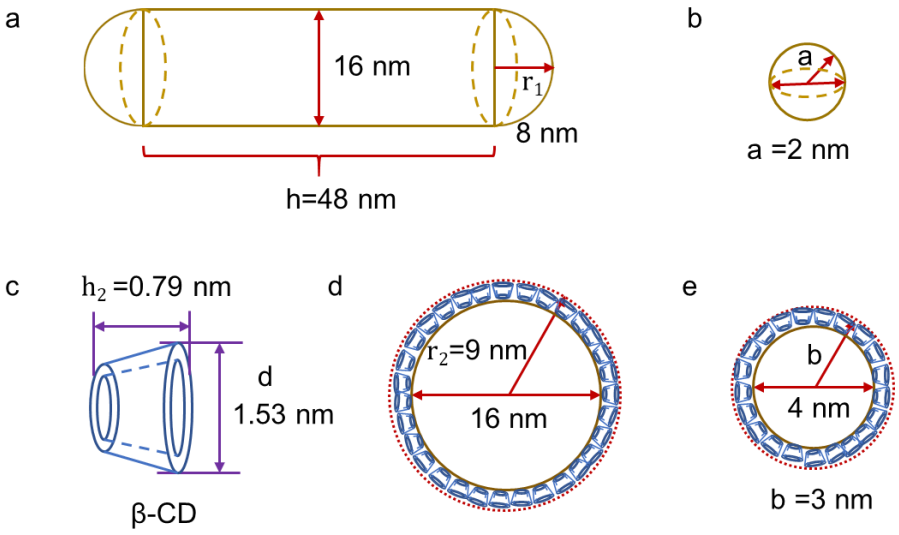

Scheme S3 Diagram of structure model of (a) AuNR, (b) gold sphere, (c) β-CD and the cross-section of (d) CD-AuNR and (e) CD-Au sphere.

In the case of CD standing on the Au surface via S-Au bond to form a fully covered monolayer, the cross-section of CD-AuNRs and CD-Au sphere can be drawn in Scheme S3d, e. Since the secondary face is larger than the primary face, the total surface area of CD is calculated according to the outer edge. Considering the length of grafting group on the rim, the distance between CD and gold surface is set as 0.21 nm. Then the specific surface area of CD-AuNR and CD-Au sphere can be obtained. From ICP-MS result, the total mass of Au (0.5808 mg) and S (0.0112 mg) in 1.0 mL of sample solution at a certain concentration is obtained. Thus, the total surface area of CD-AuNR and CD-Au sphere can be calculated from the mass of the Au and S element and the specific surface area. Correspondingly, the coverage of CD on gold surface can be estimated from the ratio of the total surface area of CD to the total surface area of CD-AuNR and CD-Au sphere. The detailed calculation is shown as follows.

mass (*AuNR*) = 98.88% × mass (*Au*)= 0.5743 mg;

mass (*Au sphere*) = 1.12% × mass (*Au*)=0.006505 mg;

Since the density (*Au*) = 19.32 g/cm^3,

volume $(AuNR)_{all}$ = $\frac{\text{mass } (AuNR)}{\text{density } (Au)}$ = 2.9723×10^{16} nm^3

volume $(Au\ sphere)_{all}$ = $\frac{\text{mass } (Au\ sphere)}{\text{density } (Au)}$ = 3.3667×10^{14} nm^3

As r_1 = 8 nm; a = 2 nm; h = 48 nm; h_2 = 0.79 nm;

r_2 = h_2 + r_1 + 0.21 nm = 9 nm; b = a + h_2 + 0.21 nm = 3 nm;

For the volume (*AuNR*) = $\pi {r_1}^2 h + \frac{4}{3}\pi {r_1}^3 = 3756.57\pi$ nm^3,

the surface area *(CD-AuNR)* = $4\pi {r_2}^2 + 2\pi r_2 h = 1188\pi$ nm^2

Likewise, the volume (*Au sphere*) = $\frac{4}{3}\pi a^3 = 10.667\pi$ nm^3,

the surface area *(CD-Au sphere)* = $4\pi b^2 = 36\pi$ nm^2

Thus,

specific surface area *(CD-AuNR)* = 0.3162 nm^{-1};

specific surface area *(CD-Au sphere)* = 3.3750 nm^{-1}

surface area $(CD\text{-}AuNR)_{all}$ =0.3162 × volume $(AuNR)_{all}$ = 9.3984×10^{15} nm^2

surface area $(CD\text{-}Au\ sphere)_{all}$ =0.8675 × volume $(Au\ sphere)_{all}$ = 1.1362×10^{15} nm^2

molar amount (*T-CD*) = $\frac{\text{mass } (T\text{-}CD)}{\text{molar mass } (T\text{-}CD)}$ = 9.6852×10^{-9} mol

number (*T-CD*) =number (*T-CD*) × N_A = 5.8323×10^{15}

surface area *(T-CD)* = $\pi(\frac{d}{2})^2 = 0.58\pi$ nm^2

surface area $(T\text{-}CD)_{all}$ = number (*T-CD*) × surface area *(T-CD)* = 1.0622×10^{16} nm^2

Therefore, the coverage of T-CDs on the surface of Au will be

$$\frac{\text{surface area } (T-CD)_{all}}{\text{surface area } (T-CD-AuNR)_{all} + \text{surface area } (T-CD-AuNS)_{all}} = 98.16\%$$

S6. Calculation of photothermal conversion efficiency.

The conditions are set when CD-AuNR or C-AuNR dispersed in aqueous solution is irradiated by an 808 nm NIR laser light with 1 W/cm^2.

Calculation of the dimensionless driving force temperature (θ).

$$\theta = \frac{T - T_0}{T_{Max} - T_0}$$

Where *T* is the solution temperature at time *t*, T_{max} is the highest temperature the solution can reach, T_0 is the starting solution temperature.

Calculation of the system heat-transfer time constant (τ_s).

$$\tau_S = -\frac{t}{ln\theta} = 528.8\ s$$

Calculation of the value of *hS.*

$$hS = \frac{\sum_i m_i C_{p,i}}{\tau_s} = 0.0127$$

Where *h* is the heat transfer coefficient, *S* is the surface area of the container, *m* is the mass of the water, *Cp* is the heat capacity of the water.

Calculation of heat released from light absorbed by container with pure water (Q_0).

$$Q_0 = \frac{cm\Delta T}{t} = 0.0434\ J \cdot s^{-1}$$

Where ΔT is the temperature drop of the pure water solution after turning off the laser, *t* is heat dissipation time of pure water.

Calculation of the photothermal conversion efficiency ($\eta_{CD-AuNR}$).

The value is obtained from the following equation based on the data in Figure S8,

$$\eta_{CD-AuNR} = \frac{hS(T_{Max} - T_0) - Q_0}{I(1 - 10^{-A_{808}})} = 51.18\%$$

where *I* is the laser lamp power ($I = 1\ W$), A_{808} is the UV absorbance of the CD-AuNR aqueous solution at 808 nm ($A_{808} = 0.7546$).

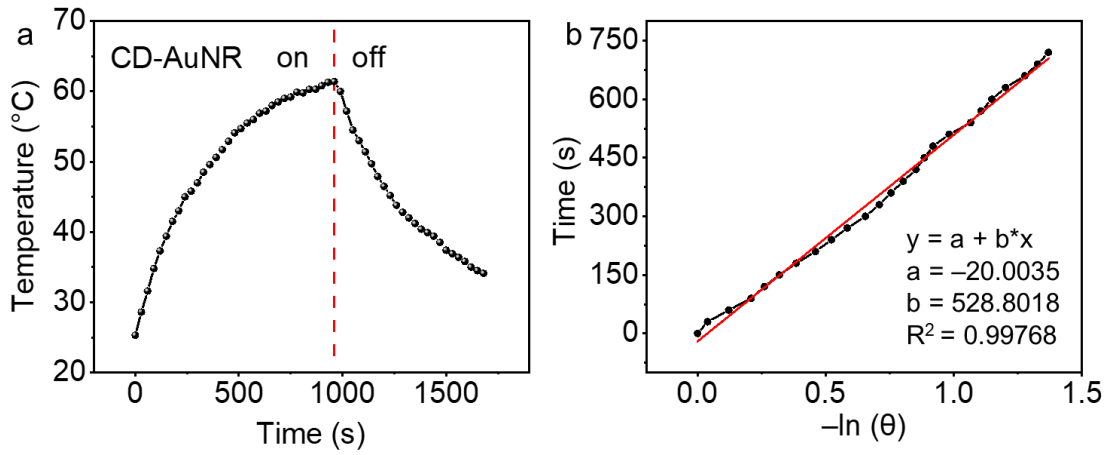

Fig. S8 (a) Temperature variation curve of CD-AuNR in aqueous solution suffering the irradiation of 808 nm laser (1.0 W/cm^2) on and off versus time and (b) the corresponding plot of time versus the –ln (θ) obtained from cooling period with fitting.

Calculation of photothermal conversion efficiency (η_{C-AuNR}).

The value is obtained from the following equation based on the data in Figure S9,

$$\eta_{C-AuNR} = \frac{hS(T_{Max} - T_0) - Q_0}{I(1 - 10^{-A_{808}})} = 51.98\%$$

where *I* is the laser lamp power ($I = 1\ W$), A_{808} is the UV absorbance of the C-AuNR aqueous solution at 808 nm ($A_{808} = 0.7611$).

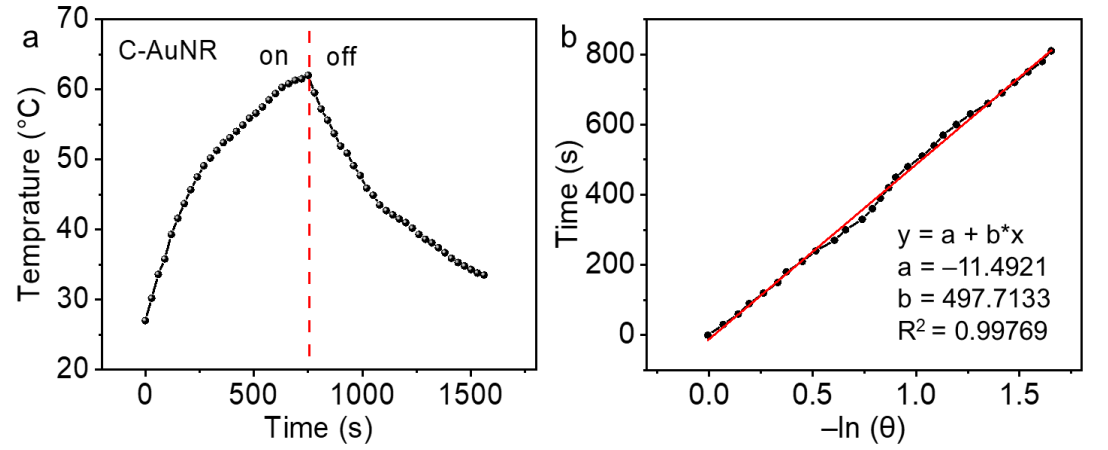

Fig. S9 (a) Temperature variation curve of C-AuNR in aqueous solution suffering the irradiation of 808 nm laser (1.0 W/cm^2) on and off versus time and (b) the corresponding plot of time versus the –ln (θ) obtained from cooling period with fitting.

S7. Characterization on NIR photothermally enhanced catalysis.

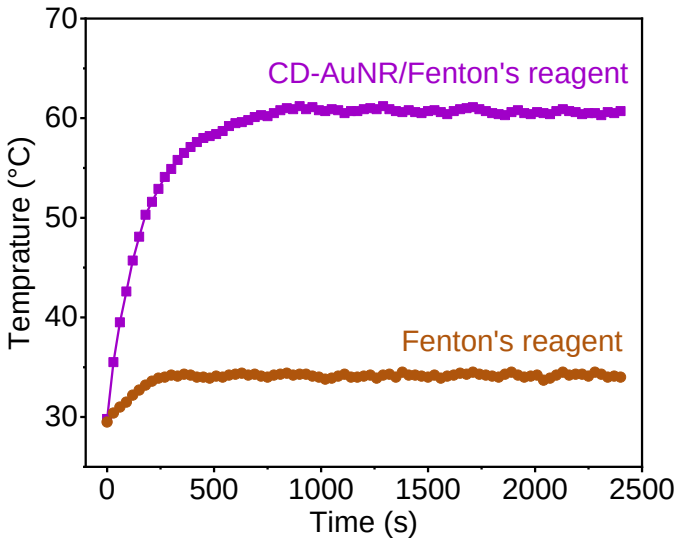

Fig. S10 The plots of temperature variation curve of the Fenton's reagent with and without CD-AuNR.

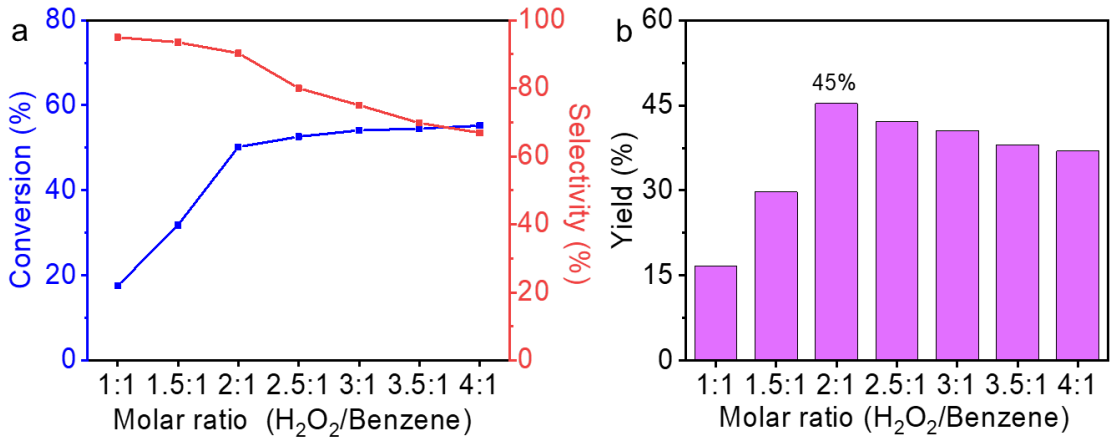

Fig. S11 (a) Conversion and selectivity plots, and (b) the yield of phenol versus the molar ratio of H_2O_2:benzene, under the reaction condition: 0.5 mL CD-AuNR aqueous solution, benzene (10 mg), 30% H_2O_2, $FeCl_3$ (0.085 mg), 30 min, irradiated by NIR light (808 nm, 1 W/cm^2).

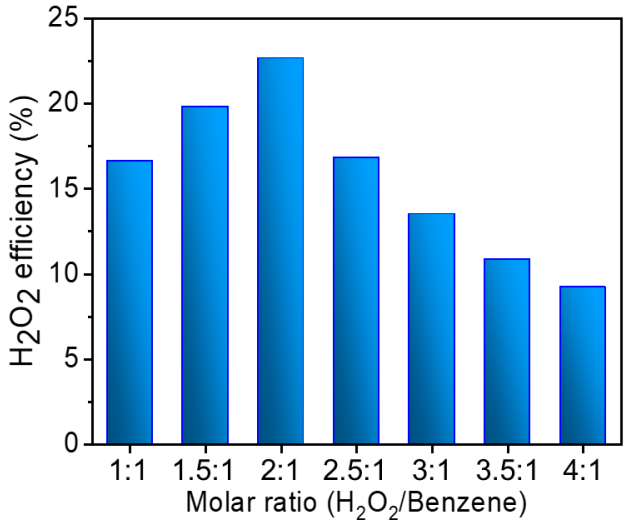

Fig. S12 Availability of H_2O_2 versus the H_2O_2:benzene molar ratio, under the reaction condition: 0.5 mL CD-AuNR aqueous solution, benzene (10 mg), 30% H_2O_2, $FeCl_3$ (0.085 mg), 30 min, irradiated by NIR light (808 nm, 1 W/cm^2).

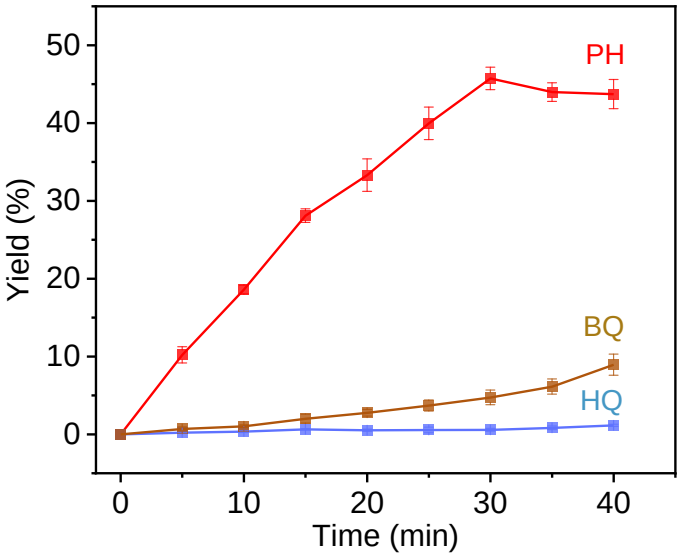

Fig. S13 Yield dependent plots of phenol (PH), benzoquinone (BQ) and hydroquinone (HQ) versus the reaction time in benzene hydroxylation catalysed by CD-AuNR/Fenton's reagent under NIR light irradiation (808 nm, 1.0 W/cm^2). Reaction conditions: benzene (10 mg), 30% H_2O_2 (34 μL), $FeCl_3$ (0.085 mg).

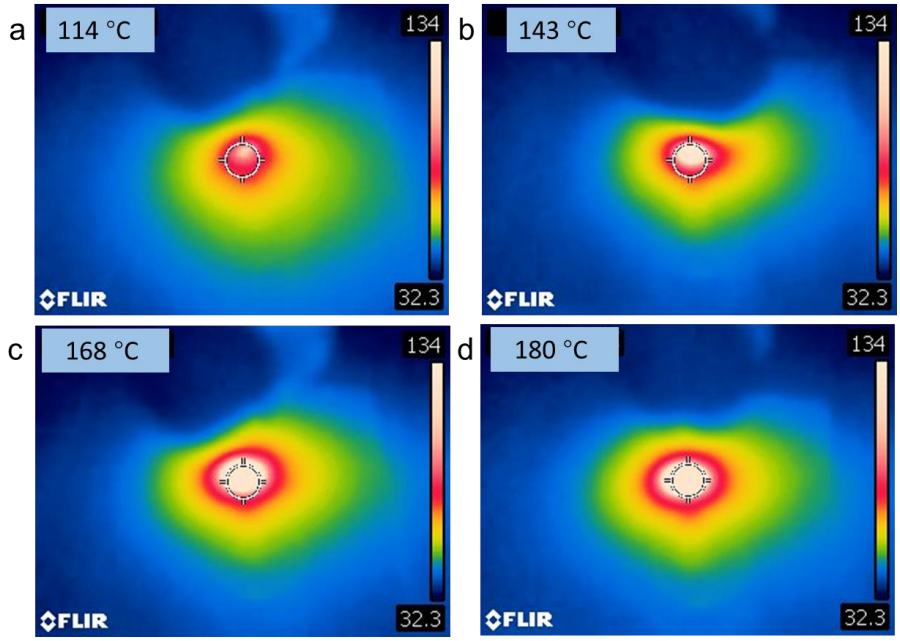

Fig. S14 NIR photographs of surface temperatures of CD-AuNR casting solid on glass under NIR laser irradiation (808 nm, 1 W/cm^2) for (a) 5 s, (b) 10 s, (c) 15 s, and (d) 20 s, detected by IR thermal camera.

Table S1. [a]The summary for benzene hydroxylation catalyzed by CD-AuNR in Fenton's solution.

Catalyst	Condition	Time/min	[b]Con./%	[b]Sel./%		
				PH	HQ	BQ
CD-AuNR ($Fe^{3+}/Cu^{2+}/H_2O_2$)	NIR (60°C)	30	60.4	75.3	5.6	20.1
CD-AuNR ($Fe^{3+}/HClO_4/H_2O_2$)	NIR (60°C)	30	6.9	61.5	11.5	26.9
CD-AuNR ($Fe^{3+}/CH_3COOH/H_2O_2$)	NIR (60°C)	30	1.5	–	–	100
CD-AuNR ($Fe^{3+}/H_2SO_4/H_2O_2$)	NIR (60°C)	30	1.0	50.0	–	50.0

[a]Reaction condition: CD-AuNR aqueous solution (0.5 mL), benzene (10 mg), 30% H_2O_2 (34 μL), $FeCl_3$ (0.085 mg), 30 min; molar ratio: 1:400:200 (cat:Sub:Ox); irradiation with NIR light (808 nm, 1 W/cm^2); [b]The results were examined by HPLC (CH_3OH: H_2O = 7:3, 0.75 mL/min). Con = conversion, Sel = selectivity.

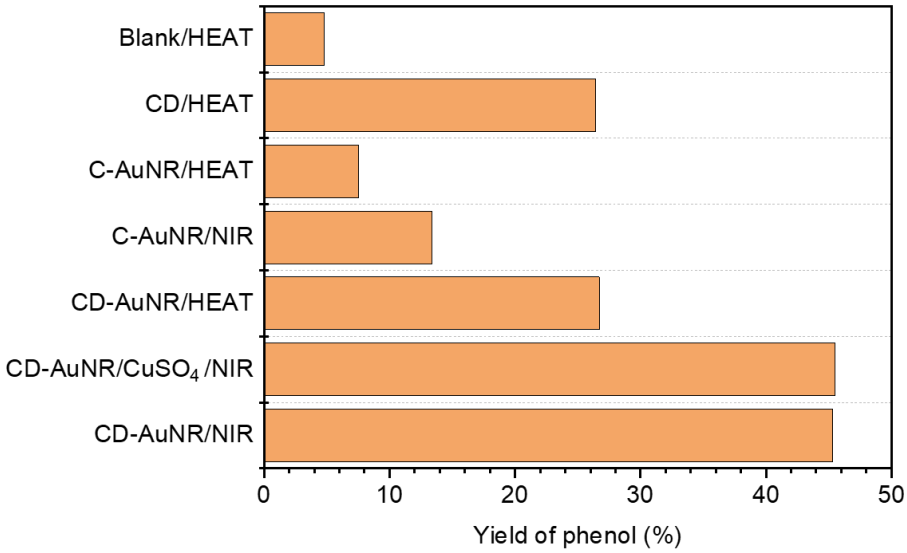

Fig. S15 Yield columns of phenol versus the additives in the presence of external heating or NIR photothermal conversion, under the condition of benzene (10 mg), 30% H_2O_2 (34 μL), $FeCl_3$ (0.085 mg), 30 min.

Table S2. The summary of benzene hydroxylation catalyzed by various iron-loaded catalysts with H_2O_2 as the oxidant under different reaction conditions.

Entry	Catalysts	Reaction conditions	Con./%	Sel./%	Yie./%	TOF/h^{-1}	Ref.
1	Fe^{II} NHC	MeCN, 25°C, 1 h.	13.0	87.0	11.3	13	3
2	Fe/GO	acetic acid, 65°C, 3 h.	15.9	94.1	15.0	7.5	4
3	MIL-100(Fe)	300 W Xe lamp, MeCN/H_2O, 25°C, 8 h.	21.7	96.0	20.8	–	5
4	iminopyridine Fe(II)	MeCN, 25°C, 1.5 h.	45.0	51.1	23.0	30	6
5	FeOCl	acetic acid, 60°C, 4 h.	43.5	100	43.5	1.2	7
6	Fe-ZSM-5	MeCN, 60°C, 8 h.	25.5	90	23.0	10.2	8
7	h-BCN_{30} (Fe^{3+}/H_2O_2)	500 W Xe lamp, MeCN/H_2O, 60°C, 2 h.	15.9	88.3	14.0	77.4	9
8	Fe@NC	MeCN, 60°C, 12h.	16.8	95	16.0	0.6	10
9	Fe–Cu/beta zeolites	MeCN, 60°C, 6h.	37.6	91	10.5	6.4	11
10	BCPOM (Fe^{2+}/H_2O_2)	acetic acid, MeCN/H_2O, 80°C, 1 h.	–	–	70	–	12
11	$FeVO_4$@TMOS	300 W Xe lamp, MeCN/H_2O, 24°C, 4 h.	20.4	98	20.0	0.3	13
12	$ZnFe_2O_4$@C	300 W Xe lamp, MeCN/H_2O, 25°C.	15.6	99.4	15.5	–	14
13	FeCo@C	MeCN/H_2O, 60°C, 4 h.	27.4	96.2	26.4	8.5	15
14	**CD-AuNR (Fe^{3+}/H_2O_2)**	**808 nm light, 1 W/cm^2, H_2O, 60°C, 0.5 h.**	**50.2**	**90.3**	**45.3**	**245.3**	**This work**

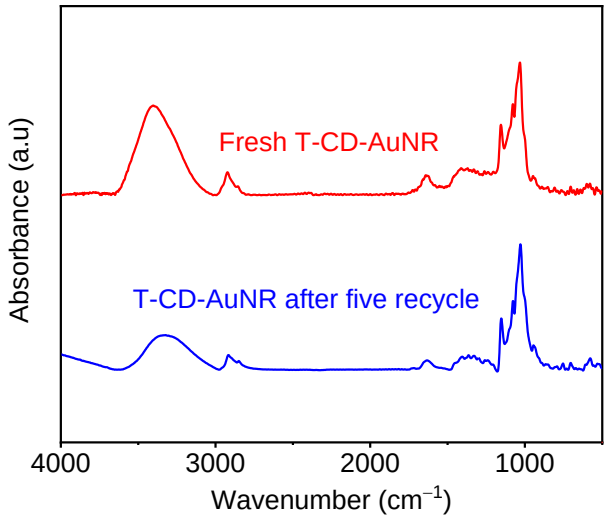

Fig. S16 FT-IR spectra of fresh CD-AuNR and recycled one after five catalytic runs in KBr pellet.

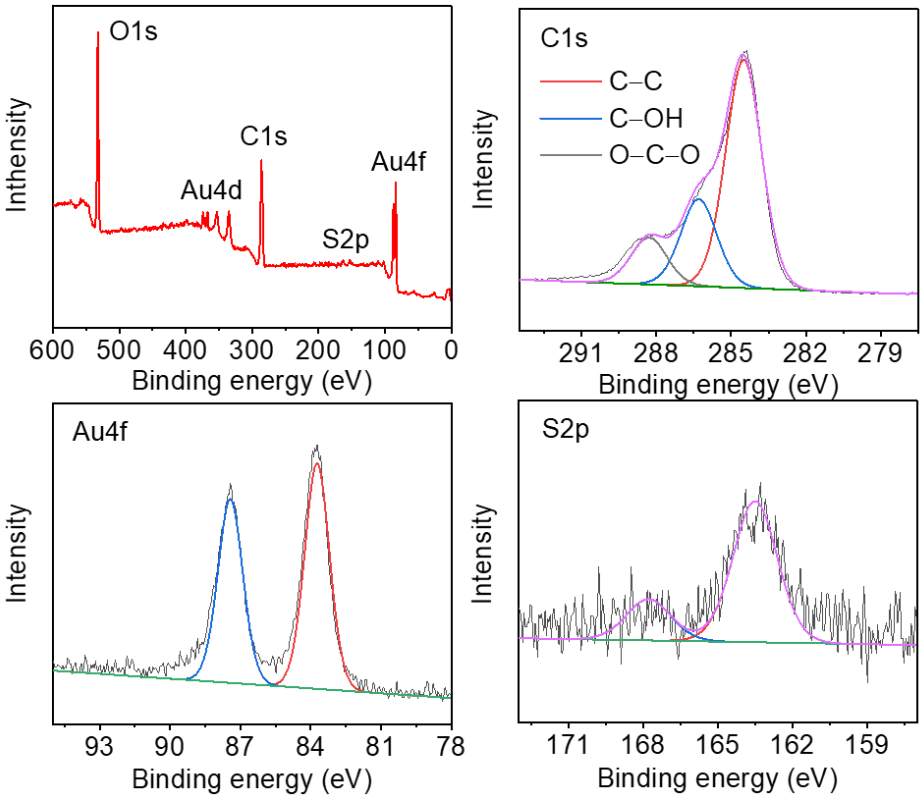

Fig. S17 XPS analysis for CD-AuNR recycled after five catalytic runs.

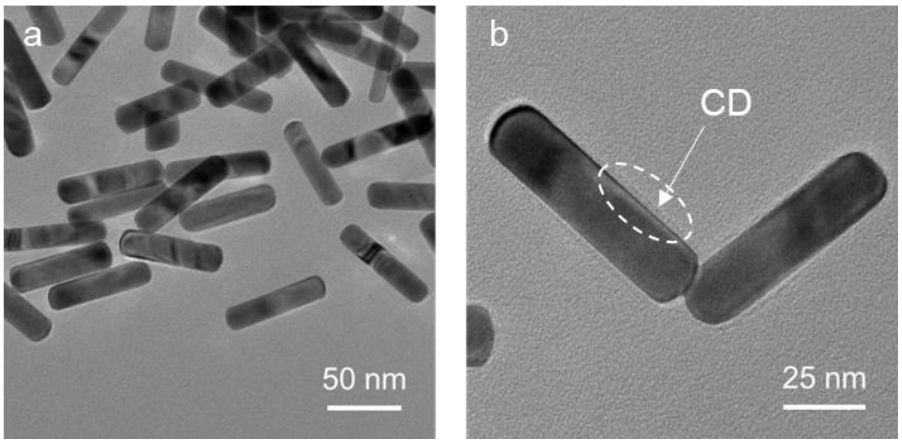

Fig. S18 TEM images of (a) recycled CD-AuNR after five catalytic runs and (b) its local magnification.

Table S3. The ICP-MS data of CD-AuNRs before and after five catalytic runs.

Element	Fresh CD-AuNR	Recycled CD-AuNR	Error
Au	580.8 ppm	570.2 ppm	1.8%
S	11.2 ppm	10.9 ppm	2.2%

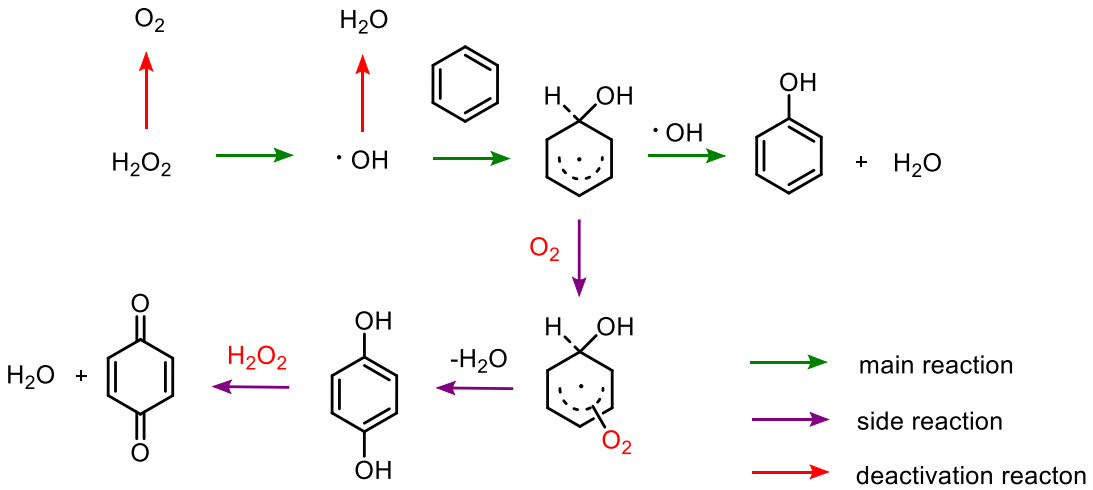

Scheme S4. Proposed mechanism of benzene hydroxylation catalyzed by Fenton's reagent mixed with CD-AuNRs under 808 nm laser light exposition.

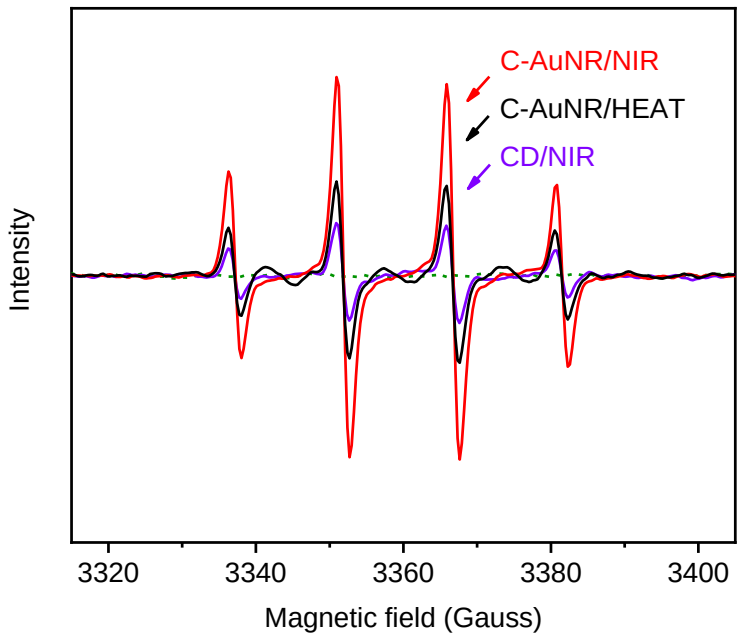

Fig. S19 DMPO spin-trapped EPR spectra of •OH radical, which is generated in C-AuNR/Fenton's reagent under NIR light irradiation (red line), external heating condition (black line) and in CD/Fenton's reagent under NIR light irradiation (purple line).

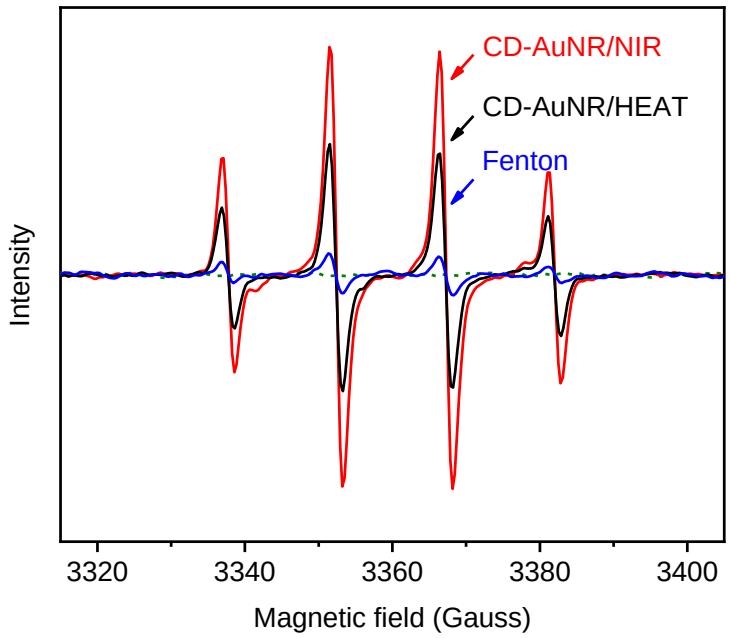

Fig. S20 DMPO spin-trapped EPR spectra of •OH radical, which is generated in CD-AuNR/Fenton's reagent under NIR light irradiation (red line), external heating condition (black line) and in Fenton's reagent under NIR light irradiation (blue line).

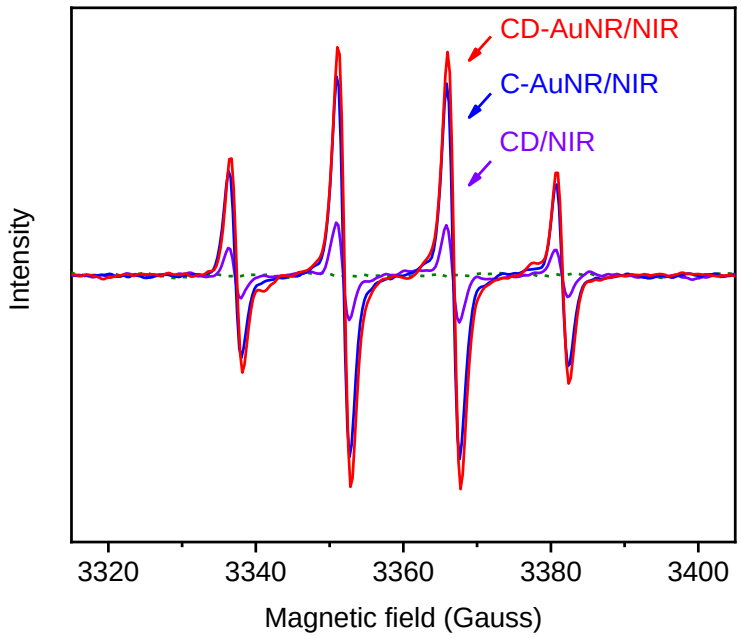

Fig. S21 DMPO spin-trapped EPR spectra of •OH radical which is generated in CD-AuNR/Fenton's reagent (red line), C-AuNR/Fenton's reagent (blue line) and in CD/Fenton's reagent (purple line) at the same concentration under NIR light irradiation.

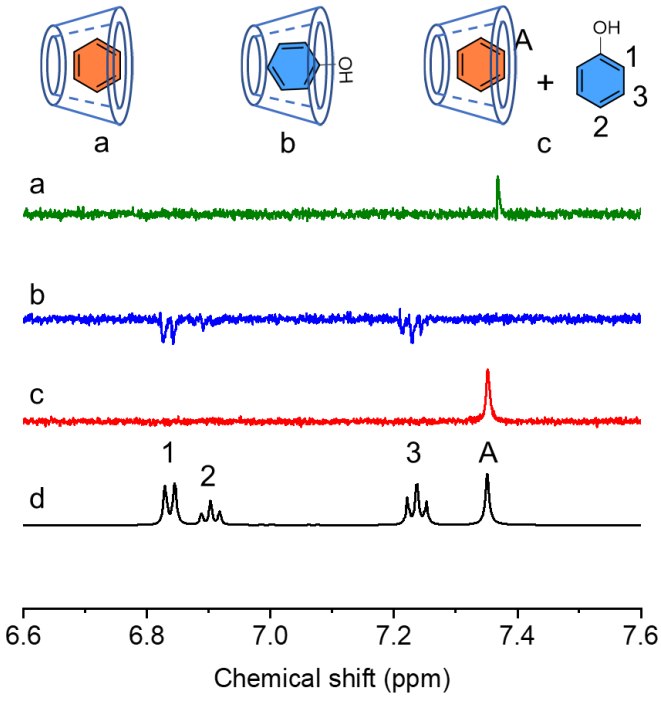

Fig. S22 1D selective gradient NOESY NMR spectra of equimolar quantities of (a) β-CD and benzene, (b) β-CD and phenol and (c) β-CD, benzene and phenol in D_2O at 25°C, under irradiation to the frequency belonging to β-CD at 3.45–3.89 ppm, and (d) ^1H NMR spectrum of equimolar quantities of β-CD, benzene, and phenol in D_2O at 25°C.

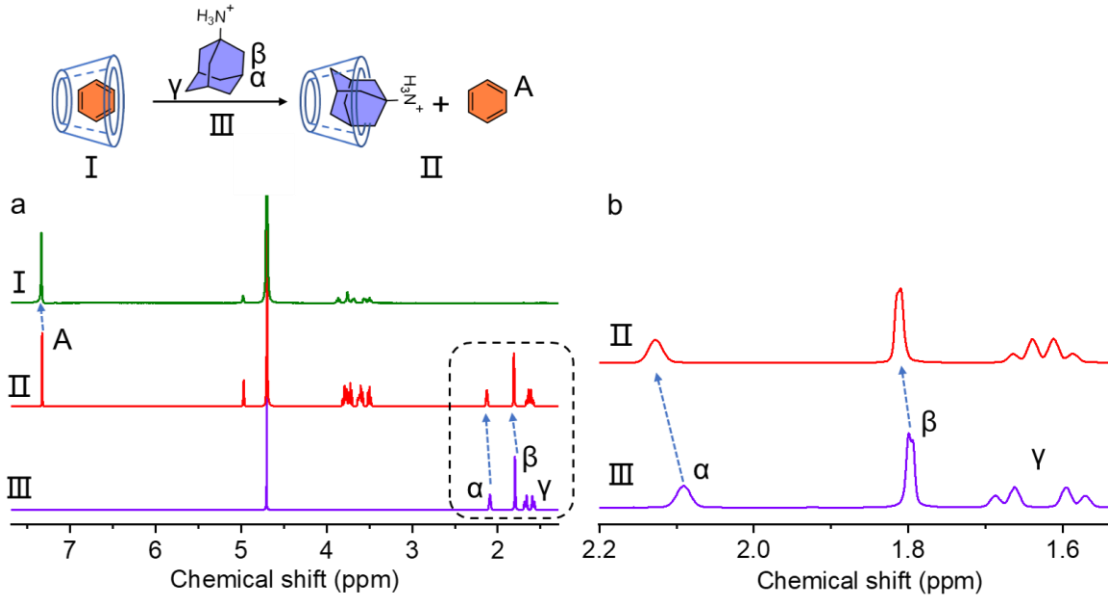

Fig. S23 ^{1}H NMR spectra of equimolar quantities of (a) β-CD and benzene (I), β-CD, benzene and adamantane hydrochloride (II) and adamantane hydrochloride (III) in D_2O at 25°C, and (b) local magnification showing the change of H_α, H_β and H_γ.

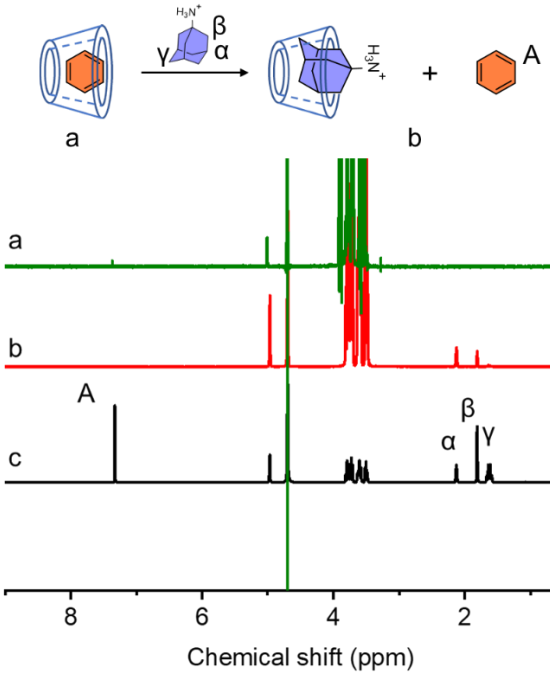

Fig. S24 Selective gradient NOESY spectra of equimolar quantities of (a) β-CD and benzene, (b) β-CD, benzene, and adamantane hydrochloride in D_2O at 25°C, which is irradiated with the frequency belonging to β-CD at 3.45–3.89 ppm, and (c) ^{1}HNMR spectrum of equimolar quantities of β-CD, benzene, and adamantane hydrochloride.

Reference

1 J. Szejtli, *Chem. Rev.*, 1998, **98**, 1743-1754.

2 A. Harada, Y. Takashima and M. Nakahata, *Acc. Chem. Res.*, 2014, **47**, 2128-2140.

3 A. Raba, M. Cokoja, W. A. Herrmann and F. E. Kuhn, *Chem. Commun.*, 2014, **50**, 11454-11457.

4 C. Wang, L. Hu, Y. Hu, Y. Ren, X. Chen, B. Yue and H. He, *Catal. Commun.*, 2015, **68**, 1-5.

5 D. Wang, M. Wang and Z. Li, *ACS Catal.*, 2015, **5**, 6852-6857.

6 G. Capocasa, G. Olivo, A. Barbieri, O. Lanzalunga and S. Di Stefano, *Catal. Sci. Technol.*, 2017, **7**, 5677-5686.

7 A. E. ElMetwally, G. Eshaq, F. Z. Yehia, A. M. Al-Sabagh and S. Kegnæs, *ACS Catal.*, 2018, **8**, 10668-10675.

8 M. Shahami, K. M. Dooley and D. F. Shantz, *J. Catal.*, 2018, **368**, 354-364.

9 B. Wang, M. Anpo, J. Lin, C. Yang, Y. Zhang and X. Wang, *Catal. Today*, 2019, **324**, 73-82.

10 E. Lu, J. Wu, B. Yang, D. Yu, Z. Yu, Y. Hou and J. Zhang, *ACS Appl. Nano Mater.*, 2020, **3**, 9192-9199.

11 P. Xiao, R. Osuga, Y. Wang, J. N. Kondo and T. Yokoi, *Catal. Sci. Technol.*, 2020, **10**, 6977-6986.

12 L. Cheng, H. Wang, H. Cai, J. Zhang, X. Gong and W. Han, *Science*, 2021, **374**, 77-81.

13 D. Wei, L. Huang, H. Liang, J. Zou, W. Chen, C. Yang, Y. Hou, D. Zheng and J. Zhang, *Catal. Sci. Technol.*, 2021, **11**, 5931-5937.

14 B. Yang, S. Zhang, Y. Gao, L. Huang, C. Yang, Y. Hou and J. Zhang, *Appl. Catal. B-Environ.*, 2022, **304**, 120999.

15 L. Zeng, H. Liang, P. An, D. Yu, C. Yang, Y. Hou and J. Zhang, *Appl. Catal. A-Gen.*, 2022, **633**, 118499.